NASA TECHNICAL REPORT

NASA TR R-448

NASA TR R-448

THE ANNULAR SUSPENSION AND POINTING (ASP) SYSTEM FOR SPACE EXPERIMENTS AND PREDICTED POINTING ACCURACIES

Willard W. Anderson and Suresh M. Joshi

Langley Research Center
Hampton, Va. 23665

NATIONAL AERONAUTICS AND SPACE ADMINISTRATION • WASHINGTON, D. C. • DECEMBER 1975

1 Report No	2 Government Accession No	3 Recipient's Catalog No
NASA TR R-448		

4 Title and Subtitle	5 Report Date
THE ANNULAR SUSPENSION AND POINTING (ASP) SYSTEM FOR SPACE EXPERIMENTS AND PREDICTED POINTING ACCURACIES	December 1975
	6 Performing Organization Code
7 Author(s)	8 Performing Organization Report No
Willard W. Anderson and Suresh M Joshi	L-10391
	10 Work Unit No
9 Performing Organization Name and Address	506-19-13-01
NASA Langley Research Center Hampton, Va 23665	11 Contract or Grant No
	13 Type of Report and Period Covered
12 Sponsoring Agency Name and Address	Technical Report
National Aeronautics and Space Administration Washington, D C 20546	14 Sponsoring Agency Code

15 Supplementary Notes

Suresh M Joshi NRC-NASA Resident Research Associate, now with Old Dominion University Research Foundation, Norfolk, Va

16 Abstract

An annular suspension and pointing (ASP) system consisting of pointing assemblies for coarse and vernier pointing is described The first assembly is attached to a carrier spacecraft (e g , the space shuttle) and consists of an azimuth gimbal and an elevation gimbal which provide "coarse" pointing The second or vernier pointing assembly is made up of magnetic actuators for suspension and fine pointing, roll motor segments, and an instrument or experiment mounting plate around which is attached a continuous annular rim similar to that used in the annular momentum control device (AMCD). The rim provides appropriate magnetic circuits for the actuators and the roll motor segments for any instrument roll position. The results of a study to determine the pointing accuracy of the system in the presence of crew motion disturbances are presented. Typical 3σ worst-case errors are found to be of the order of 0.001 arc-second.

17 Key Words (Suggested by Author(s))	18 Distribution Statement
Space shuttle spacelab Magnetic isolation and pointing Magnetic vernier pointing Experiment fine pointing	Unclassified – Unlimited Subject Category 19

19 Security Classif (of this report)	20 Security Classif (of this page)	21 No of Pages	22 Price*
Unclassified	Unclassified	34	$3 75

*For sale by the National Technical Information Service, Springfield, Virginia 22161

THE ANNULAR SUSPENSION AND POINTING (ASP) SYSTEM FOR SPACE EXPERIMENTS AND PREDICTED POINTING ACCURACIES

Willard W. Anderson and Suresh M. Joshi*
Langley Research Center

SUMMARY

An annular suspension and pointing (ASP) system consisting of pointing assemblies for coarse and vernier pointing is described. The first assembly is attached to a carrier spacecraft (e.g., the space shuttle) and consists of an azimuth gimbal and an elevation gimbal which provide "coarse" pointing. The second or vernier point assembly is made up of magnetic actuators for suspension and fine pointing, roll motor segments, and an instrument or experiment mounting plate around which is attached a continuous annular rim similar to that used in the annular momentum control device (AMCD). The rim provides appropriate magnetic circuits for the actuators and the roll motor segments for any instrument roll position. The results of a study to determine the pointing accuracy of the system in the presence of crew motion disturbances are presented. Typical 3σ worst-case errors are found to be of the order of 0 001 arc-second.

INTRODUCTION

Requirements exist for an apparatus which can provide fine pointing for a variety of solar-, stellar-, and Earth-viewing scientific instruments during extended space shuttle orbital missions. As a by-product of analytical and experimental work on an annular momentum control device (AMCD), discussed in reference 1, a concept for such an apparatus, an annular suspension and pointing (ASP) system, has been conceived. The purpose of this report is to introduce this concept, to explain the hardware configuration, and to give results of an analytical study of pointing performance in the presence of crew motion forces and moments applied to the carrier at a crew station. Disturbances caused by gravity gradient torques, aerodynamic torques, and other environmental torques were considered negligible relative to the magnitude of the crew motion disturbances. Sensor- and actuator-noise disturbances were neglected in order to determine ultimate pointing accuracies. When possible, the analysis has used normalized configuration and perfor-

*NRC-NASA Resident Research Associate, now with Old Dominion University Research Foundation, Norfolk, Va.

mance variables to simplify use of the results for arbitrary size, mass, and inertia of both the ASP system itself and the experiment or instrument mounted to it.

SYMBOLS

A, A_1, A_2	coefficient matrices
B_1, b_2, b	input matrices
$\{c\}$	vector location of center of mass of vernier pointing assembly in X_r, Y_r, Z_r system
(c_{xr}, c_{yr}, c_{zr})	components of $\{c\}$ (figs. 5 and 6)
$\{d_c\}$	displacement from carrier center of mass to intersection of coarse gimbal axes
E	expected value operator
F_{xc}, F_{yc}, F_{zc}	crew motion forces acting along X_c, Y_c, and Z_c
F_{xr}, F_{yr}, F_{zr}	magnetic bearing forces along X_r, Y_r, and Z_r
f(t)	forcing function of normalized crew motion forces and moments applied at crew station
H(s)	crew motion filter transfer function
h_1, h_2, h_3, h_4	crew motion filter state variables
I_v	inertia of vernier pointing assembly
I_{XX}, I_{YY}, I_{ZZ}	inertias of carrier about X_c, Y_c, and Z_c (subscript c has been dropped for convenience)
L	transformation matrix
M_{xc}, M_{yc}, M_{zc}	crew motion moments acting along X_c, Y_c, and Z_c
m_v	mass of vernier pointing assembly

P,P^*	origin of X_r',Y_r',Z_r' and X_r,Y_r,Z_r systems, respectively
r	radius of annular suspension system rim
s	Laplace variable
t	time
U	$= \frac{1}{c_{zr,o}^2}$
$u(t)$	$= \frac{v(t)}{c_{zr,o}}$
$v(t)$	unity power spectral density white noise
X_b,Y_b,Z_b	instrument-fixed coordinate axes
X_c,Y_c,Z_c	carrier coordinate axes
X_g,Y_g,Z_g	coarse gimbal axes
X_i,Y_i,Z_i	inertial coordinate axes with origin at carrier center of mass
X_p,Y_p,Z_p	coordinate axes parallel to X_c, Y_c, and Z_c but displaced $\{d_c\}$
X_r,Y_r,Z_r	coordinate axes displaced along Z_r' from X_r' and Y_r'
X_r',Y_r',Z_r'	coordinate axes rotated from X_g, Y_g, and Z_g through ψ_r
X_t,Y_t,Z_t	inertial coordinate axes with origin at vernier pointing assembly center of mass
x_s	complete state variable
x_1	state vector of vernier pointing assembly and carrier
x_2	state vector of crew motion filters
$\delta_{xr},\delta_{yr},\delta_{zr}$	normalized centering errors

$\delta\ell$ $= \dfrac{c_{zr} - c_{zr,o}}{c_{zr,o}}$

$\delta\epsilon$ $= \dfrac{c_{yr} - c_{yr,o}}{c_{yr,o}}$

$\delta\nu$ $= \dfrac{c_{xr} - c_{xr,o}}{c_{xr,o}}$

ϵ $= \dfrac{c_{yr}}{r}$

η^2 $= \dfrac{m_v c_{zr}^2}{I_v}$

ν $= \dfrac{c_{xr}}{r}$

ρ_i damping ratios where $i = \phi t, \theta t$, xr, yr, and zr

ρ_1, ρ_2 crew motion filter parameters

Σ covariance matrix

$\overline{\Sigma}$ steady-state covariance matrix

σ standard deviation

τ_1, τ_2 crew motion filter parameters

ϕ_c, θ_c, ψ_c carrier attitude angles

ϕ_t, θ_t vernier pointing angles

ψ_g, θ_g coarse gimbal angles

ψ_r instrument roll angle

ω_i natural frequencies where $i = \phi t, \theta t$, xr, yr, and zr

ω_1,ω_2 crew motion filter cutoff frequencies

Subscripts:

n normalized

o measured value

α ratio of actual to measured value

$\theta t,\phi t$ rotation angles of vernier pointing assembly

Superscript:

T transpose of matrix

Dots over symbols denote differentiation with respect to time.

The notation [ ] denotes a matrix.

DESCRIPTION OF ANNULAR SUSPENSION AND POINTING SYSTEM

General Description and Operational Use

The annular suspension and pointing (ASP) system includes two assemblies with connecting interfaces, each assembly having a separate function. (See fig. 1(a).) The first assembly is attached to the carrier vehicle and consists of an azimuth gimbal and an elevation gimbal which provide "coarse" pointing of the payload instrument by allowing two rotations of the instrument relative to the carrier vehicle. The second or vernier pointing assembly is made up of magnetic actuators for suspension and fine pointing, roll motor segments, and an instrument mounting plate around which a continuous annular rim is attached which provides appropriate magnetic circuits for the actuators and the roll motor segments. The vernier pointing assembly is attached to the elevation gimbal and provides vernier attitude fine pointing and roll positioning of the instrument as well as six-degree-of-freedom isolation from carrier motion disturbances. In addition, the second assembly has a rim centering mode in which axial and radial rim position sensors located at each actuator station (four stations are assumed throughout this report) are used to center the rim axially and radially between actuator pole faces. This mode allows coarse gimbal slewing for retargeting, for Earth pointing, or for backup coarse gimbal pointing.

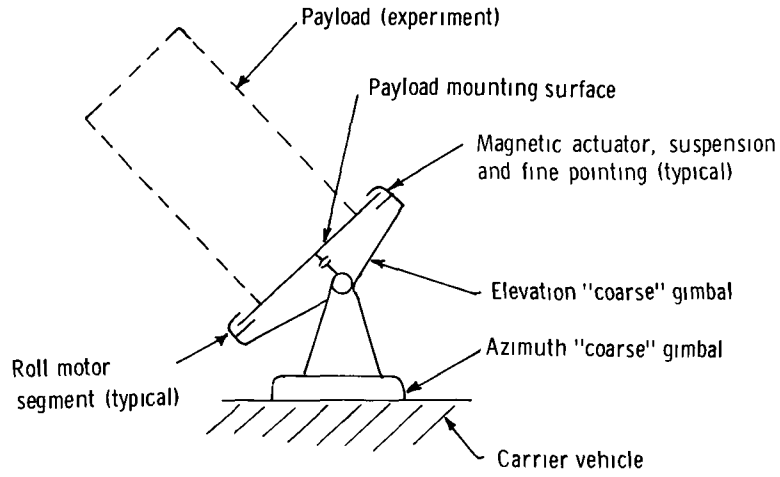

(a) Azimuth-elevation gimbal configuration.

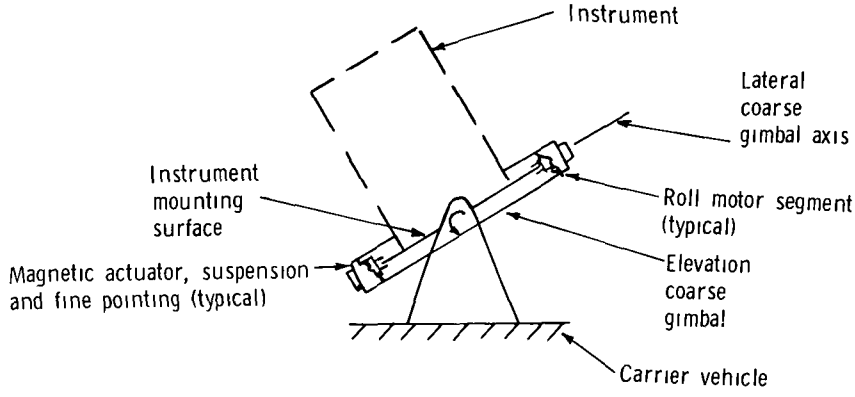

(b) Elevation-lateral gimbal configuration.

Figure 1.- Annular suspension and pointing (ASP) system.

Nominal operation of the ASP system for solar or stellar pointing first involves coarse gimbal pointing with coarse (wide field of view) sensors onboard the ASP system (or with sensors onboard the carrier vehicle and relative gimbal angle information). The rim centering mode is activated during gimbal slewing. After coarse alinement, coarse roll positioning is accomplished by means of the rim roll motor and a relative roll sensor located on the rim together with a carrier sensor or a sensor onboard the ASP system. After coarse attitude alinement, vernier fine pointing is initiated. For this mode, errors obtained from fine (narrow field of view) attitude sensors located on the ASP system, either as part of the instrument or remote, are nulled by small magnetic-suspension- and fine-pointing-actuator torques applied to the annular rim. Also, translation rim centering is accomplished for this mode.

Nominal operation of the ASP system for Earth pointing initially involves establishing the correct azimuth, elevation, and roll attitudes and attitude rates (slewing) in the rim centering mode. After appropriate smooth instrument slewing is established, vernier pointing (similar to that described for solar and stellar pointing) is accomplished. For extensive Earth pointing usage an alternative coarse gimbal arrangement (fig. 1(b)) may be preferable in which an elevation and a lateral gimbal provide simpler crosstrack capability when the carrier vehicle is in an inverted position relative to the local vertical.

Upon completion of a pointing task, connection of appropriate interfaces (data, power, cryogenic) between the payload mounting surface and the first assembly takes place. These interfaces could be maintained during a pointing task if the pointing degradation caused by the interface connection (wire, tubing, etc.) were tolerable.

Description of Coarse Gimbals

The azimuth (or lateral) and elevation gimbals which provide coarse pointing each include mechanical bearings, a torque motor, a tachometer, and a position readout potentiometer. These components interface with the control computer to form two closed-loop servosystems.

Description of Vernier Pointing Assembly

The vernier pointing assembly is shown schematically in figure 2 and is similar to the suspension system discussed in reference 1. Electromagnets (attached to the eleva-

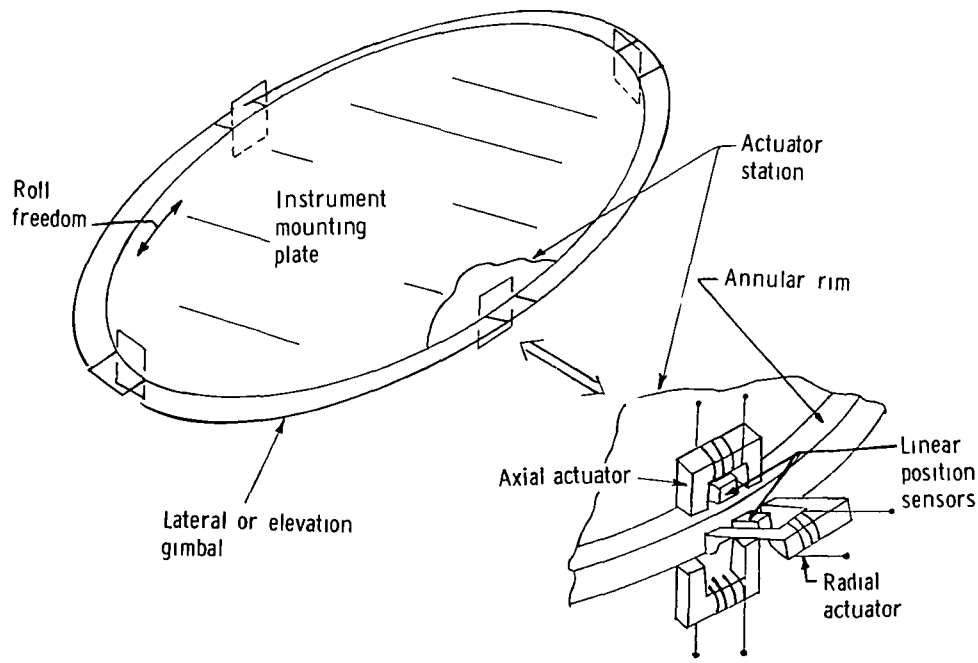

Figure 2.- Vernier pointing assembly configuration.

tion or the lateral gimbal) working in opposed pairs (both radial and axial) are used to provide fine pointing forces on the rim of the instrument mounting plate. The command forces originate from rim position sensors attached to the lateral or the elevation gimbal while in the rim centering mode or from instrument pointing error sensors for the axial actuators while in the vernier pointing mode. The radial actuators are always maintained in the rim centering mode. Roll positioning is provided by a linear noncontacting roll torque motor (not shown) which produces forces tangential to the rim. Roll angle is determined from a linear sensor located along the periphery of the rim. Thus it is seen that the instrument mounting plate is completely isolated from the elevation gimbal when there are no interface connections, and the only forces produced on it, as long as the electromagnet gaps are maintained, are those produced by the electromagnets themselves, in response to command signals.

Mission Configuration

The ASP system is shown attached to a carrier vehicle in figure 3. The vehicle is assumed to be manned, and the location of the crew station and the ASP system can be defined with reference to the principal axes X_c, Y_c, and Z_c which are a carrier-fixed coordinate system with origin at the carrier center of mass.

DESCRIPTION OF MATHEMATICAL MODEL

Coordinate Systems

The carrier and coarse gimbal coordinate systems are shown in figure 4. The system X_i,Y_i,Z_i is inertial and is nominally centered at the carrier center of mass. The system X_c,Y_c,Z_c is body fixed with origin also at the carrier center of mass. Carrier attitude is given by a set of Euler angles ϕ_c,θ_c,ψ_c with a X_c,Y_c,Z_c rotation sequence. These angles are considered small throughout this report. The system X_p,Y_p,Z_p is body fixed and is centered at the intersection P of the coarse gimbal axes which are displaced $\{d_c\}$ from the carrier center of mass. The coarse gimbal axes are defined as X_g, Y_g, and Z_g and are rotated through the azimuth angle ψ_g and the elevation angle θ_g, as shown in figure 4.

Figure 5 illustrates the vernier pointing assembly coordinates. The coordinate system X'_r,Y'_r,Z'_r with origin at P is rotated from the system X_g,Y_g,Z_g through the instrument roll angle ψ_r. Located a distance along Z'_r from P is the nominal position of the instrument mounting plate P^*, which is the origin of the coordinate system X_r,Y_r,Z_r (fig. 5). This system is parallel to X'_r,Y'_r,Z'_r. The vector $\{c\}$ locates the nominal position of the X_t,Y_t,Z_t coordinate system which is inertial and nominally parallel to the X'_r,Y'_r,Z'_r coordinate system. Finally, the system X_b,Y_b,Z_b is an instrument-fixed system, rotated from the X_t,Y_t,Z_t system by the vernier pointing angles ϕ_t and θ_t with a X_t,Y_t rotation sequence.

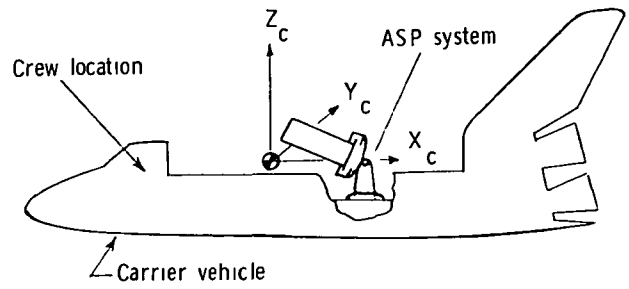

Figure 3.- Mission configuration.

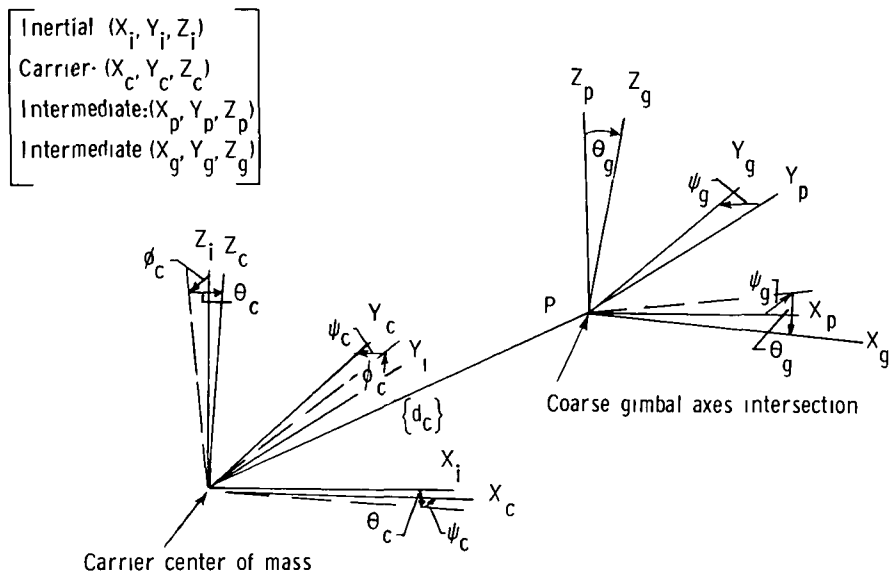

Figure 4.- Carrier and coarse gimbal coordinate systems.

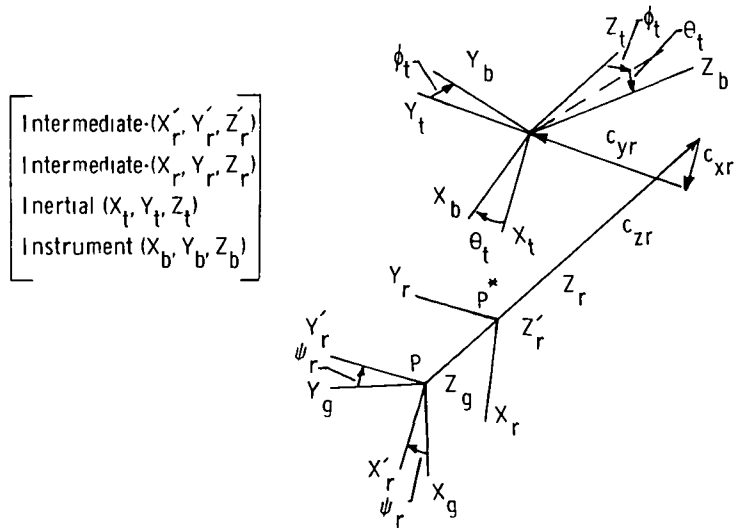

Figure 5.- Vernier pointing assembly coordinate systems.

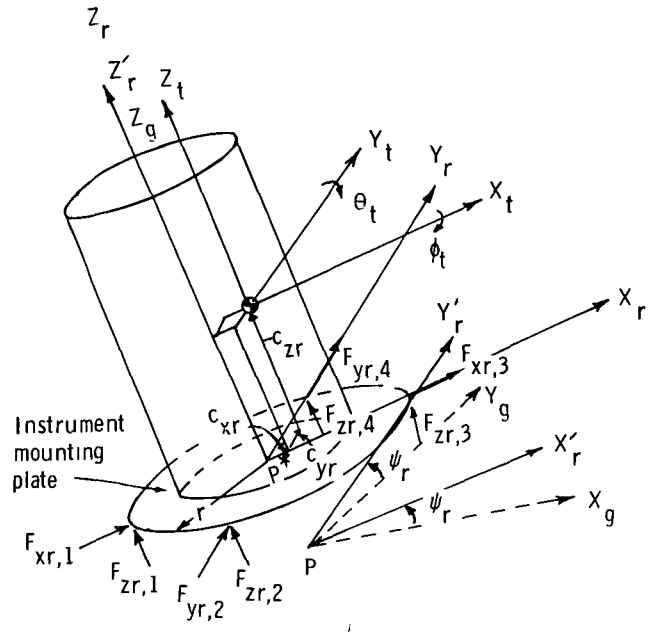

Figure 6.- Vernier pointing assembly forces.

Derivation of Mathematical Model

The mathematical model used in this report consists of two structural models. One model consists of the equations of motion of the vernier pointing assembly, and the second model consists of the equations of motion of the carrier. Lumped mass perturbation equations are derived for the vernier pointing assembly and the carrier. The vernier-pointing-assembly X_t- and Y_t-axis inertias are assumed equal. It is assumed that the motion of the vernier pointing assembly does not affect the carrier since the carrier should be much larger in inertia and mass. The carrier attitude is assumed to be controlled by such devices as control moment gyroscopes (CMG) or annular momentum control devices (AMCD). The carrier is excited by three crew motion forces and three crew motion moments acting at a crew station. The crew motion forces and moments are modeled by band-limited white-noise processes. Therefore the linearization used in modeling makes the system amenable to analysis by means of linear stochastic control theory to determine the statistical properties of various signals in the system. Only rigid-body dynamics are considered. Crew motion inertia changes are neglected.

Vernier pointing control is provided by the eight magnetic forces $F_{xr,1}$, $F_{xr,3}$, $F_{yr,2}$, $F_{yr,4}$, and $F_{zr,i}$ (i = 1, 2, 3, and 4) shown in figure 6. (Numerical subscripts refer to the four electromagnets on the rim of the instrument mounting plate.) The instrument roll control system is not shown and is not considered in the mathematical model because it does not affect the pointing accuracy in the linearized analysis. The objective of the control system is to minimize centering errors δ_{xr}, δ_{yr}, and δ_{zr} and

vernier pointing errors ϕ_t and θ_t (from offset nominal mean values). Since the analysis is linear, these mean values are taken to be zero. This is accomplished by using the magnetic forces which are synthesized as linear functions of pointing-angle errors and error rates and relative displacements and velocities between the vernier pointing assembly and the carrier (centering errors and error rates). In this study such a design, which also minimizes the norm of the control force vector, is accomplished. Detailed derivation of the equations of motion and the control system is given in the appendix. Normalization is used wherever possible in the derivation.

The equations of motion for the complete closed-loop system can be written in the following state-variable form:

$$\dot{x}_1(t) = A_1 x_1(t) + B_1 f(t) \tag{1}$$

where the 16 by 16 matrix A_1 and the 16 by 6 matrix B_1 are defined in the appendix, and the 16-dimensional state vector is

$$x_1(t) = \left(\phi_t, \dot{\phi}_t, \delta_{yr}, \dot{\delta}_{yr}, \theta_t, \dot{\theta}_t, \delta_{xr}, \dot{\delta}_{xr}, \delta_{zr}, \dot{\delta}_{zr}, \phi_{c,n}, \dot{\phi}_{c,n}, \theta_{c,n}, \dot{\theta}_{c,n}, \psi_{c,n}, \dot{\psi}_{c,n}\right)^T \tag{2}$$

where: ϕ_t and θ_t are the vernier pointing angle errors; δ_{xr}, δ_{yr}, and δ_{zr} are the centering errors normalized by the nominal Z_r-axis center-of-mass offset $c_{zr,o}$; and $\phi_{c,n}$, $\theta_{c,n}$, and $\psi_{c,n}$ are the carrier attitude angles also normalized by $c_{zr,o}$. The normalized six-dimensional crew motion disturbance vector $f(t)$ is defined as

$$f(t) = \frac{1}{c_{zr,o}}\left(F_{xc}, F_{yc}, F_{zc}, M_{xc}, M_{yc}, M_{zc}\right)^T \tag{3}$$

where F_i and M_i (i = xc, yc, and zc) are the crew motion forces and moments acting parallel to X_c, Y_c, and Z_c.

DISTURBANCE MODEL

The carrier is excited by force and moment inputs generated by the movement of the crew members at the crew station. The crew activities considered here are

(1) Console operation 1

(2) Console operation 2

(3) Hand washing

(4) Meal preparation

(5) Shaving

(6) Shower preparation

(7) Shower

(8) Secure crew shower

(9) Compressive walking

(10) Handrail

Some of these activities do not require appreciable translation of the center of mass of the crew member (e.g., console operation), whereas other activities (e.g., compressive walking and handrail) require considerable translation of the center of mass. A detailed description of each activity may be found in reference 2.

The crew motion forces and moments have been approximated by zero-mean band-limited white-noise processes in reference 2. Each crew motion force and moment is generated by passing a unit power spectral density white-noise process through a linear filter which is represented by the general transfer function (ref. 2)

$$H(s) = \frac{\tau_1 s\left(\tau_2 s + 1\right)}{\left(s^2 + 2\rho_1\omega_1 s + \omega_1{}^2\right)\left(s^2 + 2\rho_2\omega_2 s + \omega_2{}^2\right)} \tag{4}$$

Therefore a total of six filters, three for the forces and three for the moments, are required to describe the crew motion disturbances for each crew activity.

In order for the system to be amenable to analysis through application of linear stochastic control theory, it is necessary to represent this transfer function in state-space form. There are many ways to represent the above transfer function in state-variable form. One way is to write the transfer function (eq. (4)) as a cascade of two transfer functions, each having numerator dynamics. This avoids the presence of large numbers in the system matrix which can cause numerical difficulties in computing the steady-state covariance matrix. The result is

$$\frac{d}{dt}\begin{bmatrix} h_1 \\ h_2 \\ h_3 \\ h_4 \end{bmatrix} = \begin{bmatrix} 0 & 1 & 0 & 0 \\ -\omega_1{}^2 & -2\rho_1\omega_1 & 1 & \tau_2 \\ 0 & 0 & 0 & 1 \\ 0 & 0 & -\omega_2{}^2 & -2\rho_2\omega_2 \end{bmatrix}\begin{bmatrix} h_1 \\ h_2 \\ h_3 \\ h_4 \end{bmatrix} + \begin{bmatrix} 0 \\ \tau_1\tau_2 \\ \tau_1 \\ -2\rho_2\omega_2\tau_1 \end{bmatrix} v(t) \tag{5}$$

where the crew motion disturbance (force or moment) is $h_1(t)$. The crew motion filter state equations are given by

$$\dot{x}_2(t) = A_2\, x_2(t) + b_2\, u(t) \qquad f(t) = L\, x_2(t) \tag{6}$$

where x_2 is the 24 by 1 state vector of the six crew motion filters. The matrix A_2 (24 by 24) is formed by appropriate combination of the system matrices of all filters, and matrix L is the transformation from x_2 to the normalized crew motion disturbance vector $f(t)$. The scalar $u(t) = v(t)/c_{zr,o}$ is the input where $v(t)$ is a zero-mean unity power spectral density white noise Combining equations (1) and (6) yields

$$\dot{x}_S(t) = A\, x_S(t) + b\, u(t) \tag{7}$$

where

$$A = \begin{bmatrix} A_1 & B_1 L \\ 0 & A_2 \end{bmatrix} \qquad b = \begin{bmatrix} 0 \\ b_2 \end{bmatrix} \qquad x_S = \begin{bmatrix} x_1 \\ x_2 \end{bmatrix}$$

METHOD OF SOLUTION

For the above linear system (eq. (7)) excited by white noise, the evolution of the covariance matrix can be written as (see ref. 3)

$$\frac{d\Sigma(t)}{dt} = A\, \Sigma(t) + \Sigma(t)\, A^T + bUb^T \tag{8}$$

where $\Sigma(t) = E\left[x_S(t)\, x_S{}^T(t)\right]$ and $U = 1/c_{zr,o}^2$ (covariance intensity of $u(t)$). For steady state (where A is stable),

$$A\overline{\Sigma} + \overline{\Sigma}A^T + \frac{bb^T}{c_{zr,o}^2} = 0 \tag{9}$$

where $\overline{\Sigma} = \lim_{t\to\infty} \Sigma(t)$. Thus the matrix $\overline{\Sigma}c_{zr,o}^2$ can be obtained by solving the steady-state covariance equation (eq. (9)). Except for ϕ_t, $\dot{\phi}_t$, θ_t, and $\dot{\theta}_t$, all other components of the state vector x_S are normalized by $c_{zr,o}$. Thus, it is necessary to divide

the appropriate diagonal elements of $\overline{\Sigma}c_{zr,o}^2$ by $c_{zr,o}^2$ to obtain the variances of ϕ_t and θ_t. The variances of all other variables are given by the appropriate diagonal elements of $\overline{\Sigma}c_{zr,o}^2$. Since $\overline{\Sigma}$ is a symmetric matrix, equation (9) represents a system of $\frac{n}{2}(n+1)$ simultaneous linear algebraic equations where n is the dimension of A. A number of methods are available for the solution of this equation without having to invert a high dimensional matrix $\left(\text{of order } \frac{n}{2}(n+1)\right)$. In particular, the method of reference 4 was found to be efficient and accurate and was therefore used to obtain the numerical results. The control forces are simply linear transformations of the state vector; therefore the covariance matrix for the control forces can be easily obtained from $\overline{\Sigma}$.

DISCUSSION OF ANALYTICAL RESULTS

The objective of this study is to investigate the pointing performance of the ASP system when the carrier is subjected to random force and moment crew motion inputs at the crew station. To that effect a linearized model of the vernier pointing system was developed, and a pointing control system was designed on the basis of the nominal (measured) values of the parameters: $m_{v,o}$, $I_{v,o}$, $\nu_o = c_{xr,o}/r$, $\epsilon_o = c_{yr,o}/r$, $c_{zr,o}$, η_o^2, and $r/c_{zr,o}$. This model was coupled to the stabilized carrier model, which in turn was coupled to the crew motion filters excited by white noise.

In the absence of errors in the measurement of $c_{xr,o}$, $c_{yr,o}$, and $c_{zr,o}$, the steady-state standard deviations $\sigma_{\theta t} = \sqrt{E\left(\theta_t^2\right)}$ and $\sigma_{\phi t} = \sqrt{E\left(\phi_t^2\right)}$ are zero (eqs. (A18) and (A19)). However, when errors $\delta\nu$, $\delta\epsilon$, or $\delta\ell$ are present, $\sigma_{\theta t}$ and $\sigma_{\phi t}$ are no longer zero. The standard deviation of the total pointing error (for small θ_t and ϕ_t) is given by

$$\sigma_{\theta\phi} = \sqrt{\sigma_{\theta t}^2 + \sigma_{\phi t}^2}$$

Thus, it is meaningful to compute $\sigma_{\theta\phi}$ as a function of the parameters $\delta\nu$, $\delta\epsilon$, $\delta\ell$, $I_{v,\alpha}$, $m_{v,\alpha}$, η_o^2, and $r/c_{zr,o}$ and the control system parameters ρ_i and ω_i ($i = \phi t$, θt, xr, yr, and zr). For the purpose of the present study, it was decided to keep the nondimensional parameters η_o^2 and $r/c_{zr,o}$ and the control system parameters ρ_i ($i = \theta t$, ϕt, xr, yr, and zr) and ω_i ($i = \theta t$ and ϕt) fixed. It was decided to make $\omega_{xr} = \omega_{yr} = \omega_{zr} = \omega_{xyz}$ a variable, which took on various values. The values of these

parameters used in computation are given in table I. The parameters used for the carrier, including the locations of the crew station and the instrument station, were those approximating the NASA space shuttle. The carrier parameters are given in table II. As mentioned previously, 10 crew motion activities were considered. The parameters of the crew motion filters for each activity are listed in table III.

As pointed out previously, the quantity $c_{zr,o}\sigma_{\theta\phi}$ is obtained by solving the steady-state covariance equation. It was found numerically that $\sigma_{\theta\phi}$ was directly proportional to ω_{xyz}; therefore the quantity $\sigma_{\theta\phi}c_{zr,o}/\omega_{xyz}$ is suitable for computing the pointing error as a function of $\delta\epsilon$, $\delta\nu$, and $\delta\ell$. Also of interest are the centering errors δ_{xr}, δ_{yr}, and δ_{zr}. Since the matrix computed is $\overline{\Sigma}c_{zr,o}^2$ rather than $\overline{\Sigma}$, one can readily obtain the centering error standard deviations σ_{xr}, σ_{yr}, and σ_{zr} from the appropriate diagonal elements of the matrix $\overline{\Sigma}c_{zr,o}^2$. As a design ground rule the 3σ values of these variables should never exceed the magnetic actuator gap (e.g., 0.25 cm) for any crew activity. Finally, a suitable normalization for the control forces was found to be $c_{zr,o}\frac{r}{I_{v,o}}$ which results in the dimension of acceleration (m/sec^2); for example, $F_{zr,1,n} = F_{zr,1}c_{zr,o}\frac{r}{I_{v,o}}$.

In order to find worst-case errors, the coarse gimbal angles ψ_g and θ_g were given seven different (combination) values (table I). Experiments were first carried out for $\delta\epsilon = \delta\nu = 0$ for ϵ_o and ν_o ranging from -0.5 to 0.5, and $\delta\ell$ was varied from -0.1 to 0.1 (±10 percent error in measurement of c_{zr}). It was assumed that $m_{v,\alpha} = I_{v,\alpha} = 1 + \delta\ell$; that is, the same error was made in the measurements of c_{zy}, m_v, and I_v. It was found that for each crew activity and for each combination of coarse gimbal angles, the quantity $\sigma_{\theta\phi}c_{zr,o}/\omega_{xyz}$ varied almost linearly with $\delta\ell$ and was symmetric about the point $\delta\ell = 0$. Next, with $\delta\ell$, ϵ_o, and ν_o constant at various values, $\delta\epsilon$ and $\delta\nu$ were varied between -0.1 and 0.1 (±10 percent) for each coarse gimbal angle. It was found that the effect of errors in measuring the X_r and Y_r offsets ($\delta\nu$ and $\delta\epsilon$) of the center of mass of the vernier pointing assembly was rather small compared with the effect of error in measuring the Z_r offset ($\delta\ell$). For all the crew activities considered, the effect of X_r and Y_r measurement errors of up to 10 percent was to increase the pointing error by less than 20 percent; therefore, it was considered sufficient to compute $\sigma_{\theta\phi}c_{zr,o}/\omega_{xyz}$ as a function of $\delta\ell$ with $\delta\nu = \delta\epsilon = 0$ for ϵ_o and ν_o fixed at their worst-case value, 0.5.

For each coarse gimbal angle and for each ω_{xyz} considered, the quantity $\sigma_{\theta\phi}c_{zr,o}/\omega_{xyz}$ was found to be a nearly linear function of $\delta\ell$ almost symmetric about the point $\delta\ell = 0$. For a nominal design with $\bar{c}_{zr,o} = 1$ m and $\bar{\omega}_{xyz} = 0.0025$ rad/sec, $\sigma_{\theta\phi}c_{zr,o}/\omega_{xyz}$ can be normalized with respect to these nominal quantities. Therefore

the quantity $3\bar{\sigma}_{\theta\phi} = 3\sigma_{\theta\phi} \dfrac{c_{zr,o}}{\bar{c}_{zr,o}} \dfrac{\bar{\omega}_{xyz}}{\omega_{xyz}}$ with dimension arc-second is used for reporting the results. For each crew activity, and for the seven sets of coarse gimbal angles, $3\bar{\sigma}_{\theta\phi}$ lies within a band as shown in figure 7 for the activity compressive walking. The same pattern was found to exist for the rest of the crew activities. Maximum value of $\bar{\sigma}_{\theta\phi}$ occurred for $\delta\ell = 0.1$ for each crew activity. Maximum values of $3\bar{\sigma}_{\theta\phi}$ for all 10 crew activities considered in this study are given in table IV. In order to obtain the maximum 3σ pointing error for a particular case with $c_{zr,o}$ and ω_{xyz} different from the nominal values, one need only multiply $3\bar{\sigma}_{\theta\phi}$ by $\dfrac{1}{c_{zr,o}} \dfrac{\omega_{xyz}}{0.0025}$ where $c_{zr,o}$ and ω_{xyz} are the actual values. The coarse gimbal angle at which the worst pointing error occurred was different for each crew activity. The maximum pointing error occurred for the crew activity shower, for which $3\bar{\sigma}_{\theta\phi}$ was 0.001337 arc-second. For all crew

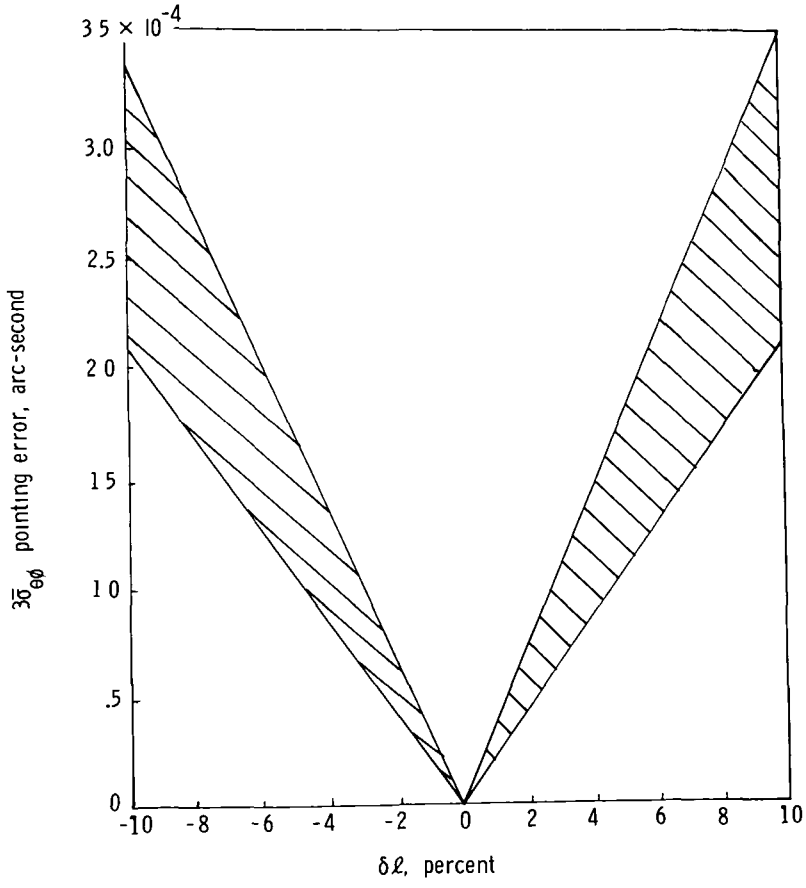

Figure 7.- 3σ pointing error for compressive walking.

activities considered, the maximum 3σ values of the centering errors $\left(3\bar{\sigma}_{xr}, 3\bar{\sigma}_{yr}, \text{and } 3\bar{\sigma}_{zr}\right)$ were well below 2.5 cm for the nominal design $\left(\overline{\omega}_{xyz} = 0.0025 \text{ rad/sec}\right)$. They were lower for higher values of $\overline{\omega}_{xyz}$. The maximum of the 3σ values of the normalized control forces $\left(\text{e.g., } F_{zr,1}c_{zr,o}r/I_{v,o}\right)$ was found to be 1.883 $\mu m/sec^2$ which occurred for the crew activity shower. The actual maximum 3σ values of the force in newtons can be obtained simply by multiplying this value by $I_{v,o}/rc_{zr,o}$.

EARTH TRACKING

In order to track a fixed point on the Earth's surface from an orbiting spacecraft, instruments mounted to the ASP system instrument mounting plate would be required to rotate relative to the carrier vehicle (assumed to rotate at orbit rate) exhibiting the bell-shaped attitude rate curve. For a 200-km orbit the peak rate can be shown to be approximately 2.2 deg/sec with peak acceleration of approximately 0.06 deg/sec^2. For an instrument inertia with respect to the coarse gimbal axes of 15 000 kg-m^2, this represents a required torque of approximately 16 N-m. It is anticipated that both the maximum rate and the maximum torque will be easily achievable with the ASP system and that Earth tracking with the ASP system, preferably with the gimbal configuration of figure 1(b), will be achievable with vernier pointing occurring simultaneously during tracking.

CONCLUSIONS

It is concluded on the basis of the steady-state analysis presented and within the assumptions presented that ultimate (perfect sensors) 3σ accuracies of an annular suspension and pointing (ASP) system are of the order of 0.001 arc-second for the cases studied. These cases were for inertial pointing (stellar targets) and crew motion disturbances. For Earth tracking it is concluded that the torques required across the vernier pointing assembly isolation gaps are easily within magnetic actuator capabilities and that simultaneous Earth tracking and vernier pointing should present no problem for the ASP system.

Langley Research Center
National Aeronautics and Space Administration
Hampton, Va. 23665
October 8, 1975

APPENDIX

DERIVATION OF EQUATIONS OF MOTION AND CONTROL SYSTEM DESIGN

In this appendix, linearized equations of motion are derived for the vernier pointing assembly and the stabilized carrier. The two models are subsequently interconnected, and a minimum-norm vernier pointing control system is derived. The equations of motion contain the three main parameters of interest: $\delta\ell = \left(c_{zr} - c_{zr,o}\right)/c_{zr,o}$, $\delta\epsilon = \left(c_{yr} - c_{yr,o}\right)/c_{yr,o}$, and $\delta\nu = \left(c_{xr} - c_{xr,o}\right)/c_{xr,o}$ where c_{xr}, c_{yr}, and c_{zr} are the coordinates of the payload instrument center of mass expressed in the coordinate system X_r,Y_r,Z_r. The subscript o denotes the measured value of the variable used for control system design. Other parameters of interest are $I_{v,\alpha} = I_v/I_{v,o}$ and $m_{v,\alpha} = m_v/m_{v,o}$, which are the ratios of the actual and the measured values of the payload inertia and mass. The main objective of the analysis is to investigate the statistical properties of the pointing accuracy when errors are present in measuring c_{xr}, c_{yr}, c_{zr}, m_v, and I_v. The control system design is based on the measured values of these quantities.

The major assumptions used in modeling were stated in the main text. As stated therein, the instrument roll control system does not affect the linearized analysis and therefore is not considered. The roll angle ψ_r is assumed to be zero. The vernier pointing system is acted on by eight forces as shown in figure 6.

Symbols

The following symbols are used in this appendix in addition to some of the symbols used and defined in the main text:

D_1 cross-product matrix of d_{xc}, d_{yc}, and d_{zc}

D_2 cross-product matrix of x_c^*, y_c^*, and z_c^*

$\left(d_{xc},d_{yc},d_{zc}\right)$ coordinates of crew station in X_c,Y_c,Z_c system

f_c normalized crew motion force vector

g_1,g_2,g_3 expressions defined in equation (A16)

I_c matrix of carrier inertias

APPENDIX

m_c mass of carrier

t_c normalized crew motion moment vector

$\left(x_c^*,y_c^*,z_c^*\right)$ coordinates of P^* in X_c,Y_c,Z_c system

$\left(x_1^*,y_1^*,z_1^*\right)$ coordinates of P^* in X_1,Y_1,Z_1 system

$\left(x_{t,cg},y_{t,cg},z_{t,cg}\right)$ center-of-mass location of vernier pointing assembly in X_t,Y_t,Z_t coordinate system

$\left(x_t^*,y_t^*,z_t^*\right)$ coordinates of point P^* fixed with respect to carrier in X_t,Y_t,Z_t system

$\left(x_t',y_t',z_t'\right)$ coordinates of the center of instrument mounting surface in X_t,Y_t,Z_t system

β_c normalized carrier attitude vector

$\delta\xi$ normalized centering error vector

Λ_β defined in equation (A24)

λ defined in equations (A10) and (A25) with appropriate subscripts

μ defined in equation (A17) with appropriate subscripts

ξ_c normalized coordinates of P^* in X_1,Y_1,Z_1 system

ξ_c^* normalized coordinates of P^* in X_t,Y_t,Z_t system

Subscripts:

$\phi c,\theta c,\psi c$ carrier attitude angles

Superscript:

-1 inverse of matrix

APPENDIX

Equations of Motion of Vernier Pointing Assembly

The dynamics of rotation for the two degrees of freedom are

$$I_v\ddot{\phi}_t = F_{zr,4}\left(r - c_{yr}\right) - F_{zr,2}\left(r - c_{yr}\right) - \left(F_{zr,1} + F_{zr,3}\right)c_{yr} + \left(F_{yr,2} + F_{yr,4}\right)c_{zr} \tag{A1}$$

$$I_v\ddot{\theta}_t = F_{zr,1}\left(r + c_{xr}\right) - F_{zr,3}\left(r - c_{xr}\right) + \left(F_{zr,2} + F_{zr,4}\right)c_{xr} - \left(F_{xr,1} + F_{xr,3}\right)c_{zr} \tag{A2}$$

The translation of the center of mass of the vernier pointing assembly is given by

$$\ddot{x}_{t,cg} = \frac{1}{m_v}\left(F_{xr,1} + F_{xr,3}\right) \tag{A3}$$

$$\ddot{y}_{t,cg} = \frac{1}{m_v}\left(F_{yr,2} + F_{yr,4}\right) \tag{A4}$$

$$\ddot{z}_{t,cg} = \frac{1}{m_v}\left(F_{zr,1} + F_{zr,2} + F_{zr,3} + F_{zr,4}\right) \tag{A5}$$

where $x_{t,cg}$, $y_{t,cg}$, and $z_{t,cg}$ are coordinates of the center of mass expressed in the X_t,Y_t,Z_t system.

When θ_t and ϕ_t are small, the coordinates of the center of the instrument mounting surface are given in the X_t,Y_t,Z_t system by

$$x_t' = x_{t,cg} - c_{zr}\theta_t$$

$$y_t' = y_{t,cg} + c_{zr}\phi_t$$

$$z_t' = z_{t,cg} - c_{zr}$$

Substitution of equations (A3), (A4), and (A5) in these equations yields

$$\ddot{x}_t' = \frac{1}{m_v}\left(F_{xr,1} + F_{xr,3}\right) - c_{zr}\ddot{\theta}_t \tag{A6}$$

$$\ddot{y}_t' = \frac{1}{m_v}\left(F_{yr,2} + F_{yr,4}\right) + c_{zr}\ddot{\phi}_t \tag{A7}$$

$$\ddot{z}_t' = \frac{1}{m_v}\left(F_{zr,1} + F_{zr,2} + F_{zr,3} + F_{zr,4}\right) \tag{A8}$$

Controller Design

The desired behavior of θ_t, ϕ_t, x_t', y_t', and z_t' can be written in the following form:

$$\left.\begin{aligned} &\ddot{x}_t' = -\lambda_{xr} \qquad \ddot{y}_t' = -\lambda_{yr} \qquad \ddot{z}_t' = -\lambda_{zr} \\ &\ddot{\phi}_t = -\lambda_{\phi t} \qquad \ddot{\theta}_t = -\lambda_{\theta t} \end{aligned}\right\} \tag{A9}$$

where

$$\left.\begin{aligned} \lambda_{xr} &= 2\rho_{xr}\omega_{xr}\left(\dot{x}_t' - \dot{x}_t^*\right) + \omega_{xr}^2\left(x_t' - x_t^*\right) \\ \lambda_{\phi t} &= 2\rho_{\phi t}\omega_{\phi t}\dot{\phi}_t + \omega_{\phi t}^2\phi_t \end{aligned}\right\} \tag{A10}$$

where ρ_{xr}, $\rho_{\phi t}$, ω_{xr}, and $\omega_{\phi t}$ are the desired damping ratios and natural frequencies; and x_t^* is the x_t-component of the position of the corresponding point P^* fixed relative to the carrier transformed to the coordinate system X_t, Y_t, Z_t. The quantities λ_{yr}, λ_{zr}, and $\lambda_{\theta t}$ are similarly defined. One way of designing a control system is to ignore the coupling from θ_t and ϕ_t to x_t' and y_t' while designing x_t' and y_t' loops. This retains the ease in the analytical treatment of the system. Design of the z_t' loop poses no coupling problem. From equations (A6), (A7), and (A8) let

$$F_{xr,1} + F_{xr,3} = -m_{v,o}\lambda_{xr} \tag{A11}$$

$$F_{yr,2} + F_{yr,4} = -m_{v,o}\lambda_{yr} \tag{A12}$$

$$F_{zr,1} + F_{zr,2} + F_{zr,3} + F_{zr,4} = -m_{v,o}\lambda_{zr} \tag{A13}$$

APPENDIX

The remaining equations for designing θ_t and ϕ_t loops allow exact compensation. From equations (A1) and (A2),

$$F_{zr,4}\left(r - c_{yr,o}\right) - F_{zr,2}\left(r + c_{yr,o}\right) - \left(F_{zr,1} + F_{zr,3}\right)c_{yr,o} + \left(F_{yr,2} + F_{yr,4}\right)c_{zr,o} = -I_{v,o}\lambda_{\phi t} \tag{A14}$$

$$F_{zr,1}\left(r + c_{xr,o}\right) - F_{zr,3}\left(r - c_{xr,o}\right) + \left(F_{zr,2} + F_{zr,4}\right)c_{xr,o} - \left(F_{xr,1} + F_{xr,3}\right)c_{zr,o} = -I_{v,o}\lambda_{\theta t} \tag{A15}$$

Equations (A13), (A14), and (A15) can be rewritten in the following form:

$$\begin{bmatrix} 1 & \nu_o & 0 & \nu_o \\ 0 & -\epsilon_o & 1 & -\epsilon_o \\ 0 & 1 & 0 & 1 \end{bmatrix} \begin{bmatrix} F_1 \\ F_2 \\ F_3 \\ F_4 \end{bmatrix} = \begin{bmatrix} -\frac{I_{v,o}}{r}\left(\lambda_{\theta t} + \eta_o{}^2\mu_{xr}\right) \\ -\frac{I_{v,o}}{r}\left(\lambda_{\phi t} - \eta_o{}^2\mu_{yr}\right) \\ -\frac{I_{v,o}}{r}\left(\frac{r}{c_{zr,o}}\right)\eta_o{}^2\mu_{zr} \end{bmatrix} = \begin{bmatrix} g_1 \\ g_2 \\ g_3 \end{bmatrix} \tag{A16}$$

where

$$\left.\begin{aligned} F_1 &= F_{zr,1} - F_{zr,3} & \eta_o{}^2 &= \frac{m_{v,o}c_{zr,o}^2}{I_{v,o}} \\ F_2 &= F_{zr,1} + F_{zr,3} & \mu_{xr} &= \frac{1}{c_{zr,o}}\lambda_{xr} \\ F_3 &= F_{zr,4} - F_{zr,2} & \mu_{yr} &= \frac{1}{c_{zr,o}}\lambda_{yr} \\ F_4 &= F_{zr,4} + F_{zr,2} & \mu_{zr} &= \frac{1}{c_{zr,o}}\lambda_{zr} \end{aligned}\right\} \tag{A17}$$

These are three linear equations in four unknowns, and more than one solution exists for this problem. The solution which minimizes the norm $\left(F_1{}^2 + F_2{}^2 + F_3{}^2 + F_4{}^2\right)^{1/2}$

and which equivalently minimizes $\left(F_{zr,1}^2 + F_{zr,2}^2 + F_{zr,3}^2 + F_{zr,4}^2\right)^{1/2}$ can be obtained by using the pseudoinverse to get

$$F_1 = g_1 - \nu_o g_3 \qquad F_2 = F_4 = \frac{1}{2} g_3 \qquad F_3 = g_2 + \epsilon_o g_3$$

Substitution of these expressions into equations (A1), (A2), (A6), (A7), and (A8) and simplification yield

$$\ddot{\phi}_t = -\frac{1}{I_{v,\alpha}} \lambda_\phi - \frac{\eta_o^2}{I_{v,\alpha}} \delta\ell\, \mu_{yr} + \frac{\eta_o^2}{I_{v,\alpha}} \epsilon_o \left(\frac{r}{c_{zr,o}}\right) \delta\epsilon\, \mu_{zr} \tag{A18}$$

$$\ddot{\theta}_t = -\frac{1}{I_{v,\alpha}} \lambda_{\theta_t} + \frac{\eta_o^2}{I_{v,\alpha}} \delta\ell\, \mu_{xr} - \frac{\eta_o^2}{I_{v,\alpha}} \nu_o \left(\frac{r}{c_{zr,o}}\right) \delta\nu\, \mu_{zr} \tag{A19}$$

$$\frac{\ddot{x}_t'}{c_{zr,o}} = -\frac{1}{m_{v,\alpha}} \mu_{xr} - (1 + \delta\ell)\ddot{\theta}_t \tag{A20}$$

$$\frac{\ddot{y}_t'}{c_{zr,o}} = -\frac{1}{m_{v,\alpha}} \mu_{yr} + (1 + \delta\ell)\ddot{\phi}_t \tag{A21}$$

$$\frac{\ddot{z}_t'}{c_{zr,o}} = -\frac{1}{m_{v,\alpha}} \mu_{zr} \tag{A22}$$

Equations of Motion of Carrier

The carrier equations of motion consist of three degrees of freedom of translation and three degrees of freedom of rotation. The carrier attitude is assumed to be stabilized by control moment gyroscopes (CMG). The equations of motion for the stabilized rotational dynamics are

$$\ddot{\beta}_c = I_c^{-1} t_c - \Lambda_\beta + I_c^{-1} D_1 f_c \tag{A23}$$

where $\beta_c = \frac{1}{c_{zr,o}} \left(\phi_c, \theta_c, \psi_c\right)^T$ is the normalized carrier attitude vector and

$$\Lambda_\beta = \frac{1}{c_{zr,o}} \left(\lambda_{\phi c}, \lambda_{\theta c}, \lambda_{\psi c}\right) \tag{A24}$$

where

$$\lambda_{\phi c} = 2\rho_{\phi c}\omega_{\phi c}\dot{\phi}_c + \omega_{\phi c}^2\phi_c \tag{A25}$$

with $\rho_{\phi c}$ and $\omega_{\phi c}$ being the desired carrier damping ratio and natural frequency. The quantities $\lambda_{\theta c}$ and $\lambda_{\psi c}$ are similarly defined. The matrix of carrier inertias is defined by

$$I_c = \begin{bmatrix} I_{XX} & 0 & 0 \\ 0 & I_{YY} & 0 \\ 0 & 0 & I_{ZZ} \end{bmatrix}$$

Finally,

$$D_1 = \begin{bmatrix} 0 & -d_{zc} & d_{yc} \\ d_{zc} & 0 & -d_{xc} \\ -d_{yc} & d_{xc} & 0 \end{bmatrix} \qquad f_c = \frac{1}{c_{zr,o}}\begin{bmatrix} F_{xc} \\ F_{yc} \\ F_{zc} \end{bmatrix} \qquad t_c = \frac{1}{c_{zr,o}}\begin{bmatrix} M_{xc} \\ M_{yc} \\ M_{zc} \end{bmatrix}$$

where (d_{xc},d_{yc},d_{zc}) are the coordinates of the crew station expressed in the system X_c,Y_c,Z_c.

The dynamics of the translation of point P^* fixed relative to the carrier consist of (1) a component due to the translation of the carrier center of mass and (2) a component due to the rotation of the carrier and the displacement of the point P^* from the carrier center of mass. These are given by

$$\ddot{\xi}_c = -D_2 I_c^{-1} t_c + D_2 \Lambda_\beta - D_2 I_c^{-1} D_1 f_c + \frac{1}{m_c} f_c \tag{A26}$$

where $\xi_c = \frac{1}{c_{zr,o}}\left(x_i^*, y_i^*, z_i^*\right)^T$ is the normalized coordinate vector of P^* expressed in the inertial system X_i,Y_i,Z_i and

$$D_2 = \begin{bmatrix} 0 & -z_c^* & y_c^* \\ z_c^* & 0 & -x_c^* \\ -y_c^* & x_c^* & 0 \end{bmatrix}$$

where (x_c^*,y_c^*,z_c^*) are the coordinates of point P^* expressed in the carrier-fixed system X_c,Y_c,Z_c and m_c is the mass of the carrier.

APPENDIX

The position of P^*, which is fixed relative to the carrier, in coordinate system X_t,Y_t,Z_t can be obtained by premultiplying ξ_c by the matrix $R = R_2(\theta_g)R_1(\psi_g)$ where

$$R_1(\psi_g) = \begin{bmatrix} \cos\psi_g & \sin\psi_g & 0 \\ -\sin\psi_g & \cos\psi_g & 0 \\ 0 & 0 & 1 \end{bmatrix} \qquad R_2(\theta_g) = \begin{bmatrix} \cos\theta_g & 0 & -\sin\theta_g \\ 0 & 1 & 0 \\ \sin\theta_g & 0 & \cos\theta_g \end{bmatrix}$$

where θ_g and ψ_g are coarse gimbal pointing angles as shown in figure 4. The instrument roll angle ψ_r is assumed to be zero. Thus $\xi_c^* = R\xi_c = \frac{1}{c_{zr,o}}\left(x_t^*, y_t^*, z_t^*\right)^T$ is the representation of the position of a suspension point fixed on the carrier in the coordinate system X_t,Y_t,Z_t.

The final step is to interconnect the vernier pointing system model to the carrier model. It has been assumed that the vernier pointing system does not affect carrier dynamics. The interconnection is done by premultiplying equation (A26) by R and subtracting the result from equations (A20), (A21), and (A22). This gives

$$\delta\ddot{\xi} = -\frac{1}{m_{v,\alpha}}\begin{bmatrix} \mu_{xr} \\ \mu_{yr} \\ \mu_{zr} \end{bmatrix} + (1 + \delta\ell)\begin{bmatrix} -\ddot{\theta}_t \\ \ddot{\phi}_t \\ 0 \end{bmatrix} + RD_2I_c^{-1}t_c$$

$$- RD_2\Lambda_\beta + RD_2I_c^{-1}D_1f_c - \frac{1}{m_c}Rf_c \qquad \text{(A27)}$$

where

$$\delta\xi = \left(\delta_x, \delta_y, \delta_z\right)^T = \left(\frac{x_t' - x_t^*}{c_{zr,o}}, \frac{y_t' - y_t^*}{c_{zr,o}}, \frac{z_t' - z_t^*}{c_{zr,o}}\right)^T$$

The complete closed-loop equations therefore consist of equations (A18), (A19), (A23), and (A27). This is a set of 16 linear constant coefficient differential equations with 6 forcing functions which are the components of the vector f, where

$$f = \frac{1}{c_{zr,o}}\left(F_{xc}, F_{yc}, F_{zc}, M_{xc}, M_{yc}, M_{zc}\right)^T$$

These equations can be written in the form of the following state-space model:

$$\dot{x}_1(t) = A_1 x_1(t) + B_1 f(t) \qquad \text{(A28)}$$

where the state vector $x_1(t)$ is defined in the main text (eq. (2)). The matrix A_1 is

APPENDIX

$$
\begin{bmatrix}
0 & 1 & 0 & 0 & 0 & 0 & 0 & 0 & 0 & 0 & 0 & 0 & 0 & 0 \\
-\frac{b_{\phi t}}{I_{v,\alpha}} & -\frac{a_{\phi t}}{I_{v,\alpha}} & -P_1 b_{yr} & 0 & 0 & 0 & Q_1 b_{zr} & Q_1 a_{zr} & 0 & 0 & 0 & 0 & 0 & 0 \\
0 & 0 & 0 & 0 & 0 & 0 & 0 & 0 & 0 & 0 & 0 & 0 & 0 & 0 \\
-\frac{\ell_\alpha b_{\phi t}}{I_{v,\alpha}} & -\frac{\ell_\alpha a_{\phi t}}{I_{v,\alpha}} & -\frac{b_{yr}}{m_{v,\alpha}} - P_1 \ell_\alpha b_{yr} & -\frac{a_{yr}}{m_{v,\alpha}} - P_1 \ell_\alpha a_{yr} & 0 & 0 & \ell_\alpha Q_1 b_{zr} & \ell_\alpha Q_1 a_{zr} & G_{21}{}^{b}{}_{\phi c} & G_{21}{}^{a}{}_{\phi c} & G_{22}{}^{b}{}_{\theta c} & G_{22}{}^{a}{}_{\theta c} & G_{23}{}^{b}{}_{\psi c} & G_{23}{}^{a}{}_{\psi c} \\
0 & 0 & 0 & 0 & 0 & 1 & 0 & 0 & 0 & 0 & 0 & 0 & 0 & 0 \\
0 & 0 & 0 & 0 & -\frac{b_{\theta t}}{I_{v,\alpha}} & -\frac{a_{\theta t}}{I_{v,\alpha}} & P_1 b_{xr} & P_1 a_{xr} & Q_2 b_{zr} & Q_2 a_{zr} & 0 & 0 & 0 & 0 \\
0 & 0 & 0 & 0 & 0 & 0 & 0 & 1 & 0 & 0 & 0 & 0 & 0 & 0 \\
0 & 0 & 0 & 0 & \frac{\ell_\alpha b_{\theta t}}{I_{v,\alpha}} & \frac{\ell_\alpha a_{\theta t}}{I_{v,\alpha}} & -\frac{b_{xr}}{m_{v,\alpha}} - \ell_\alpha P_1 b_{xr} & -\frac{a_{xr}}{m_{v,\alpha}} - \ell_\alpha P_1 a_{xr} & -\ell_\alpha Q_2 b_{zr} & -\ell_\alpha Q_2 a_{zr} & G_{11}{}^{b}{}_{\phi c} & G_{11}{}^{a}{}_{\phi c} & G_{12}{}^{b}{}_{\theta c} & G_{12}{}^{a}{}_{\theta c} & G_{13}{}^{b}{}_{\psi c} & G_{13}{}^{a}{}_{\psi c} \\
0 & 0 & 0 & 0 & 0 & 0 & 0 & 0 & 1 & 0 & 0 & 0 & 0 & 0 \\
0 & 0 & 0 & 0 & 0 & 0 & 0 & 0 & -\frac{b_{zr}}{m_{v,\alpha}} & -\frac{a_{zr}}{m_{v,\alpha}} & G_{31}{}^{b}{}_{\phi c} & G_{31}{}^{a}{}_{\phi c} & G_{32}{}^{b}{}_{\theta c} & G_{32}{}^{a}{}_{\theta c} & G_{33}{}^{b}{}_{\psi c} & G_{33}{}^{a}{}_{\psi c} \\
0 & 0 & 0 & 0 & 0 & 0 & 0 & 0 & 0 & 0 & 1 & 0 & 0 & 0 & 0 & 0 \\
0 & 0 & 0 & 0 & 0 & 0 & 0 & 0 & 0 & 0 & -b_{\phi c} & -a_{\phi c} & 0 & 0 & 0 & 0 \\
0 & 0 & 0 & 0 & 0 & 0 & 0 & 0 & 0 & 0 & 0 & 0 & 1 & 0 & 0 & 0 \\
0 & 0 & 0 & 0 & 0 & 0 & 0 & 0 & 0 & 0 & 0 & 0 & -b_{\theta c} & -a_{\theta c} & 0 & 0 \\
0 & 0 & 0 & 0 & 0 & 0 & 0 & 0 & 0 & 0 & 0 & 0 & 0 & 0 & 0 & 1 \\
0 & 0 & 0 & 0 & 0 & 0 & 0 & 0 & 0 & 0 & 0 & 0 & 0 & 0 & -b_{\psi c} & -a_{\psi c}
\end{bmatrix}
$$

APPENDIX

The matrix B_1 is

$$\begin{bmatrix}
0 & 0 & 0 & 0 & 0 & 0 \\
0 & 0 & 0 & 0 & 0 & 0 \\
0 & 0 & 0 & 0 & 0 & 0 \\
H_{21} & H_{22} & H_{23} & J_{21} & J_{22} & J_{23} \\
0 & 0 & 0 & 0 & 0 & 0 \\
0 & 0 & 0 & 0 & 0 & 0 \\
0 & 0 & 0 & 0 & 0 & 0 \\
H_{11} & H_{12} & H_{13} & J_{11} & J_{12} & J_{13} \\
0 & 0 & 0 & 0 & 0 & 0 \\
H_{31} & H_{32} & H_{33} & J_{31} & J_{32} & J_{33} \\
0 & 0 & 0 & 0 & 0 & 0 \\
K_{11} & K_{12} & K_{13} & 1/I_{XX} & 0 & 0 \\
0 & 0 & 0 & 0 & 0 & 0 \\
K_{21} & K_{22} & K_{23} & 0 & 1/I_{YY} & 0 \\
0 & 0 & 0 & 0 & 0 & 0 \\
K_{31} & K_{32} & K_{33} & 0 & 0 & 1/I_{ZZ}
\end{bmatrix}$$

The numerical subscripts to G, H, J, and K refer to i,j elements of these matrices and

$$\left.\begin{array}{lll}
P_1 = \dfrac{\eta_o^2\,\delta\ell}{I_{v,\alpha}} & Q_1 = \dfrac{\eta_o^2}{I_{v,\alpha}}\,\epsilon_o\left(\dfrac{r}{c_{zr,o}}\right)\delta\epsilon & Q_2 = -\dfrac{\eta_o^2}{I_{v,\alpha}}\,\nu_o\left(\dfrac{r}{c_{zr,o}}\right)\delta\nu \\
\ell_\alpha = 1 + \delta\ell & a_{\phi t} = 2\rho_{\phi t}\omega_{\phi t} & b_{\phi t} = \omega_{\phi t}^2
\end{array}\right\} \qquad \text{(A29)}$$

The quantities $a_{\theta t}$, $b_{\theta t}$, a_{xr}, b_{xr}, a_{yr}, b_{yr}, a_{zr}, and b_{zr} and the carrier attitude coefficients $a_{\phi c}$, $b_{\phi c}$, $a_{\theta c}$, $b_{\theta c}$, $a_{\psi c}$, and $b_{\psi c}$ are similarly defined. Finally,

$$\left.\begin{aligned} G &= -RD_2 \\ H &= \left(-\frac{1}{m_c} R + RD_2 I_c^{-1} D_1\right) \\ J &= RD_2 I_c^{-1} \\ K &= I_c^{-1} D_1 \end{aligned}\right\} \tag{A30}$$

The matrices A_1 and B_1 depend on the parameters η_o^2, $\frac{r}{c_{zr,o}}$, $\epsilon_o = \frac{c_{yr,o}}{r}$, $\nu_o = \frac{c_{xr,o}}{r}$, $\delta\ell$, $\delta\epsilon$, $\delta\nu$, $m_{v,\alpha}$, and $I_{v,\alpha}$. The last five represent per unit errors in measuring the payload parameters.

REFERENCES

1. Anderson, Willard W.; and Groom, Nelson J.: The Annular Momentum Control Device (AMCD) and Potential Applications. NASA TN D-7866, 1975.

2. Hendricks, T. C.; and Johnson, C. H.: Stochastic Crew Motion Modeling. J. Spacecraft & Rockets, vol. 8, no. 2, Feb. 1971, pp. 150-154.

3. Sage Andrew P.: Optimum Systems Control. Prentice-Hall, Inc., c.1968.

4. Smith, P. G.: Numerical Solution of the Matrix Equation $AX + XA^T + B = 0$. IEEE Trans. Automat. Contr., vol. AC-16, no. 3, June 1971, pp. 278-279.

TABLE I.- SYSTEM PARAMETERS

Direction	Natural frequency, ω	Damping ratio, ρ
θ_t	1 Hz	0.7
ϕ_t	1 Hz	.7
x_r	0.0025, 0.005, 0.01 rad/sec	.7
y_r	0.0025, 0.001, 0.01 rad/sec	.7
z_r	0.0025, 0.005, 0.01 rad/sec	.7

ψ_g, deg	θ_g, deg
0	0
0	-45
0	-75
45	-45
45	-90
90	-45
90	-90
$\eta_o^2 = 3$	

TABLE II.- CARRIER PARAMETERS

Mass, kg	82 750
Principal inertias:	
I_{XX}, kg-m^2	1 004 700
I_{YY}, kg-m^2	7 740 400
I_{ZZ}, kg-m^2	7 892 200
Crew station coordinates in X_C,Y_C,Z_C system, m	(-16.002, 0, 0.594)
Pointing-system location in X_C,Y_C,Z_C system (coordinates of P^*), m	(2.055, 0, 1.649)
Attitude control system parameters:	
Damping ratios	0.5
Natural frequencies, rad/sec	1

TABLE III.- CREW MOTION FILTER PARAMETERS

No.	Crew motion	Input	Axis	τ_1, sec	ω_1, rad/sec	ρ_1	τ_2, sec	ω_2,[a] rad/sec	ρ_2[a]
1	Console operation 1	Force	X_c	18.2773	4.0291	0.5056	0	0	0
			Y_c	17.1199	2.8065	.5565	0	0	0
			Z_c	11 400.7578	4.7634	.5986	0	31.2563	.2357
		Moment	X_c	9.8581	4.4158	0.3196	0	0	0
			Y_c	17.3380	4.0384	.4683	0	0	0
			Z_c	4.0227	4.4132	.5589	0	0	0
2	Console operation 2	Force	X_c	27.7506	4.8027	0.6176	0	0	0
			Y_c	24.9955	3.9640	.4660	0	0	0
			Z_c	24.9720	5.3108	.7719	0	0	0
		Moment	X_c	18.7626	4.5882	0.4845	0	0	0
			Y_c	28.1691	4.3448	.6750	0	0	0
			Z_c	8.0293	5.3496	.7691	0	0	0
3	Hand washing	Force	X_c	17.4926	4.6501	1.0548	0	0	0
			Y_c	3 275.9965	4.8057	.2875	0	18.3715	.1562
			Z_c	26.5141	6.6369	1.1417	0	0	0
		Moment	X_c	17.4379	7.1214	0.7451	0	0	0
			Y_c	12.8624	4.2945	.6632	0	0	0
			Z_c	6.0225	7.8253	.6068	0	0	0
4	Meal preparation	Force	X_c	17.3321	4.6927	0.6694	0	0	0
			Y_c	11 045.5850	6.2733	.9834	0	25.2278	.4105
			Z_c	18.1345	7.5724	.7760	0	0	0
		Moment	X_c	6 541.9406	5.8366	0.9194	0	24.6604	0.4224
			Y_c	16.1670	4.1801	.7043	0	0	0
			Z_c	5.2055	6.4015	.5881	0	0	0
5	Shaving	Force	X_c	20.3714	5.1021	0.8819	0	0	0
			Y_c	17.3637	11.3510	.4634	0	0	0
			Z_c	35.0996	10.9388	.4946	0	0	0
		Moment	X_c	8 307.3984	2.9119	1.0000	0	17.6599	0.5391
			Y_c	15.7655	4.8075	.7559	0	0	0
			Z_c	5.2847	6.5419	.7066	0	0	0

[a]If $\omega_2 = \rho_2 = 0$, the term $\left(s^2 + 2\rho_2\omega_2 s + \omega_2^2\right)$ is deleted from equation (4).

TABLE III.- Concluded

No.	Crew motion	Input	Axis	τ_1, sec	ω_1, rad/sec	ρ_1	τ_2, sec	ω_2,[a] rad/sec	ρ_2[a]
6	Shower preparation	Force	X_c	30.1921	3.3087	0.6553	0	0	0
			Y_c	32.3592	3.9074	.6868	0	0	0
			Z_c	69.5387	5.3796	.3319	0	0	0
		Moment	X_c	16.2769	4.5319	0.5639	0	0	0
			Y_c	27.2968	2.9091	.5955	0	0	0
			Z_c	5.9979	4.3660	.6051	0	0	0
7	Shower	Force	X_c	19.4974	3.7860	0.5581	0	0	0
			Y_c	0	2.6670	1.0000	0	9.3832	0.6828
			Z_c	100.1676	5.1450	.4474	0	0	0
		Moment	X_c	6 138.9781	1.6088	1.0000	0	8.5289	0.4883
			Y_c	16.9998	3.5191	.5352	0	0	0
			Z_c	5.7852	3.9034	.5210	0	0	0
8	Secure crew shower	Force	X_c	22.1929	4.0563	0.5220	0	0	0
			Y_c	1 235.3875	4.3531	.2397	0	11.3617	0
			Z_c	135.8161	6.9337	.5158	0	0	0
		Moment	X_c	6 388.1024	2.3809	1.0000	0	9.7396	0.6505
			Y_c	20.6119	3.1956	.6203	0	0	0
			Z_c	6.7518	3.8145	.4713	0	0	0
9	Compressive walking	Force	X_c	5.5280	4.7567	0.2097	0	0	0
			Y_c	1 672.0922	14.0260	.2601	0.0700	2.9387	.3831
			Z_c	32.3250	8.0629	.4509	0	0	0
		Moment	X_c	1 262.4496	1.2705	0.2509	0	13.3204	0.1231
			Y_c	2 856.4276	4.0364	.3839	0	16.9327	.3196
			Z_c	646.0391	2.7191	.3386	0	13.0889	.1850
10	Handrail	Force	X_c	2 060.7139	3.1361	0.5272	0	8.7844	0.1422
			Y_c	962.8141	1.7543	.6112	0	12.6152	.2416
			Z_c	20.6236	4.7574	.3170	0	0	0
		Moment	X_c	1 673.8328	4.1064	0.4465	0	19.1331	0.4519
			Y_c	724.0498	1.7012	.6911	0	8.1117	.2106
			Z_c	926.2022	1.7304	.7469	0	14.4657	.4447

[a]If $\omega_2 = \rho_2 = 0$, the term $\left(s^2 + 2\rho_2\omega_2 s + \omega_2^2\right)$ is deleted from equation (4).

TABLE IV.- MAXIMUM 3σ POINTING ERRORS

No.	Crew activity	$3\bar{\sigma}_{\theta\phi}$, arc-second
1	Console operation 1	$6\ 287 \times 10^{-4}$
2	Console operation 2	5.829
3	Hand washing	2 012
4	Meal preparation	2 652
5	Shaving	2.309
6	Shower preparation	1.097×10^{-3}
7	Shower	1.337
8	Secure crew shower	1.063
9	Compressive walking	$3\ 475 \times 10^{-4}$
10	Handrail	9.83

NASA-Langley, 1975 L-10391

NATIONAL AERONAUTICS AND SPACE ADMINISTRATION
WASHINGTON, D C 20546

OFFICIAL BUSINESS
PENALTY FOR PRIVATE USE $300

SPECIAL FOURTH-CLASS RATE
BOOK

POSTAGE AND FEES PAID
NATIONAL AERONAUTICS AND
SPACE ADMINISTRATION
451

U.S.MAIL

POSTMASTER If Undeliverable (Section 158
Postal Manual) Do Not Return

"The aeronautical and space activities of the United States shall be conducted so as to contribute . . . to the expansion of human knowledge of phenomena in the atmosphere and space. The Administration shall provide for the widest practicable and appropriate dissemination of information concerning its activities and the results thereof."

—NATIONAL AERONAUTICS AND SPACE ACT OF 1958

NASA SCIENTIFIC AND TECHNICAL PUBLICATIONS

TECHNICAL REPORTS. Scientific and technical information considered important, complete, and a lasting contribution to existing knowledge

TECHNICAL NOTES Information less broad in scope but nevertheless of importance as a contribution to existing knowledge.

TECHNICAL MEMORANDUMS Information receiving limited distribution because of preliminary data, security classification, or other reasons Also includes conference proceedings with either limited or unlimited distribution.

CONTRACTOR REPORTS Scientific and technical information generated under a NASA contract or grant and considered an important contribution to existing knowledge

TECHNICAL TRANSLATIONS Information published in a foreign language considered to merit NASA distribution in English

SPECIAL PUBLICATIONS Information derived from or of value to NASA activities Publications include final reports of major projects, monographs, data compilations, handbooks, sourcebooks, and special bibliographies

TECHNOLOGY UTILIZATION PUBLICATIONS Information on technology used by NASA that may be of particular interest in commercial and other non-aerospace applications Publications include Tech Briefs, Technology Utilization Reports and Technology Surveys.

Details on the availability of these publications may be obtained from:

SCIENTIFIC AND TECHNICAL INFORMATION OFFICE

NATIONAL AERONAUTICS AND SPACE ADMINISTRATION

Washington, D.C. 20546